ACS OMEGA

Open Access

http://pubs.acs.org/journal/acsodf

Article

Guided Design of Efficient Oxygen Evolution Catalysts Using Patent Analysis

Weiwei Zhang,[#] Yongzhi Zhao,[#] Jiali Xu, Baorui Jia,[*] Wujun Zhang,[*] and Mingli Qin[*]

Cite This: *ACS Omega* 2024, 9, 18160−18168

Read Online

ACCESS | Metrics & More | Article Recommendations | Supporting Information

ABSTRACT: The facile and rapid design of efficient oxygen evolution reaction (OER) catalysts holds paramount significance for energy conversion devices, such as water electrolyzers and fuel cells. Despite substantial progress in catalyst synthesis and performance exploration, the design and selection processes remain inefficient. In this context, we integrate patent analysis with catalyst design, leveraging the scholarly research functionalities within patent analyses to aid in the design and synthesis of a NiFeRu-carbon catalyst as a high-performance OER catalyst. The results demonstrate that the NiFeRu-Carbon catalyst with low Ru loading (0.3 wt %) exhibits an overpotential of only 219 mV at 10 mA cm^{-2} under alkaline conditions, and after continuous operation for 200 h, the overpotential only attenuates by 15 mV. The incorporation of high-valence Ru dopants elevated the intrinsic activity of individual catalytic sites within NiFe-layered double hydroxides (LDHs). During the catalytic process, the partial dissolution of Ru might lead to the generation of numerous oxygen vacancies within NiFe- LDH, thereby enhancing the catalyst's activity and stability.

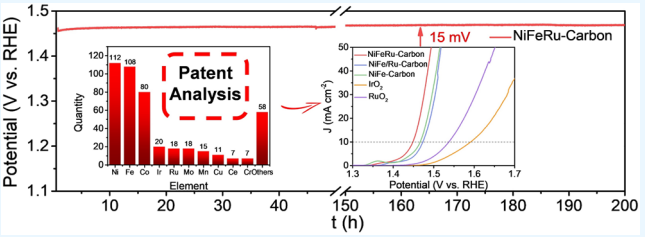

1. INTRODUCTION

The Oxygen Evolution Reaction (OER) is a pivotal reaction occurring in energy conversion and storage devices such as water electrolysis,[1−3] fuel cells,[4−6] metal-air batteries,[7−10] and others.[11−13] Therefore, the design and development of efficient OER catalysts have significant implications for enhancing energy conversion efficiency and promoting the advancement of renewable energy sources. The development of highly active and stable OER catalysts typically necessitates rational material selection and design.[14,15] Although empirical trends have been explored in practice, lengthy research cycles and intricate procedures have diminished the research efficiency. Therefore, there is an urgent need for an auxiliary strategy to facilitate the efficient design and synthesis of the catalysts.

The exploration of the journal literature frequently serves as a crucial avenue for individuals to comprehend the methodologies of catalyst preparation. Meanwhile, patents, serving as instruments for innovation and research and development, often go unnoticed, as they play a dual role in safeguarding intellectual property rights and facilitating technological exchange and dissemination.[16−18] Patent analysis (PA), on the other hand, constitutes a method for studying patent documents with the aim of extracting valuable information and data from patent databases. Through patent analysis, individuals can gain insight into the research landscape within a specific domain. Stoffels et al.,[17] utilizing patent analysis, identified a transition in heterogeneous catalytic techniques for hydrogenation reactions toward nontoxic elements, while noble metals continue to dominate homogeneous catalytic methodologies.

Here, we conduct an analysis of recently disclosed OER catalyst patents, and based on catalyst type, composition, preparation methods, etc., we anticipate that carbon-supported catalysts loaded with Ni, Fe, and Ru exhibit remarkable OER catalytic activity. We further demonstrate the facile synthesis of a composite material comprising Ni, Fe, and Ru coloaded onto a carbon cloth support (NiFeRu-Carbon) through a one-step hydrothermal approach. The results demonstrate that NiFeRu-Carbon exhibits a remarkably low overpotential of 219 mV at 10 mA cm^{-2} in alkaline conditions, with only a 15 mV decay in overpotential after 200 h of sustained operation. The utilization of a one-step hydrothermal process and a low Ru loading (0.3 wt %) contribute to cost-effectiveness. Subsequent analysis of the catalyst after stability testing reveals that the dissolution of Ru may generate a substantial number of oxygen vacancies, thereby enhancing the activity and stability of the NiFe-layered double hydroxides (LDH). This work introduces a novel approach to the design and fabrication of OER catalysts.

Received: December 20, 2023
Revised: March 27, 2024
Accepted: March 29, 2024
Published: April 12, 2024

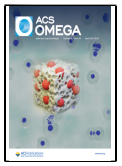

https://doi.org/10.1021/acsomega.3c10195
ACS Omega 2024, 9, 18160−18168

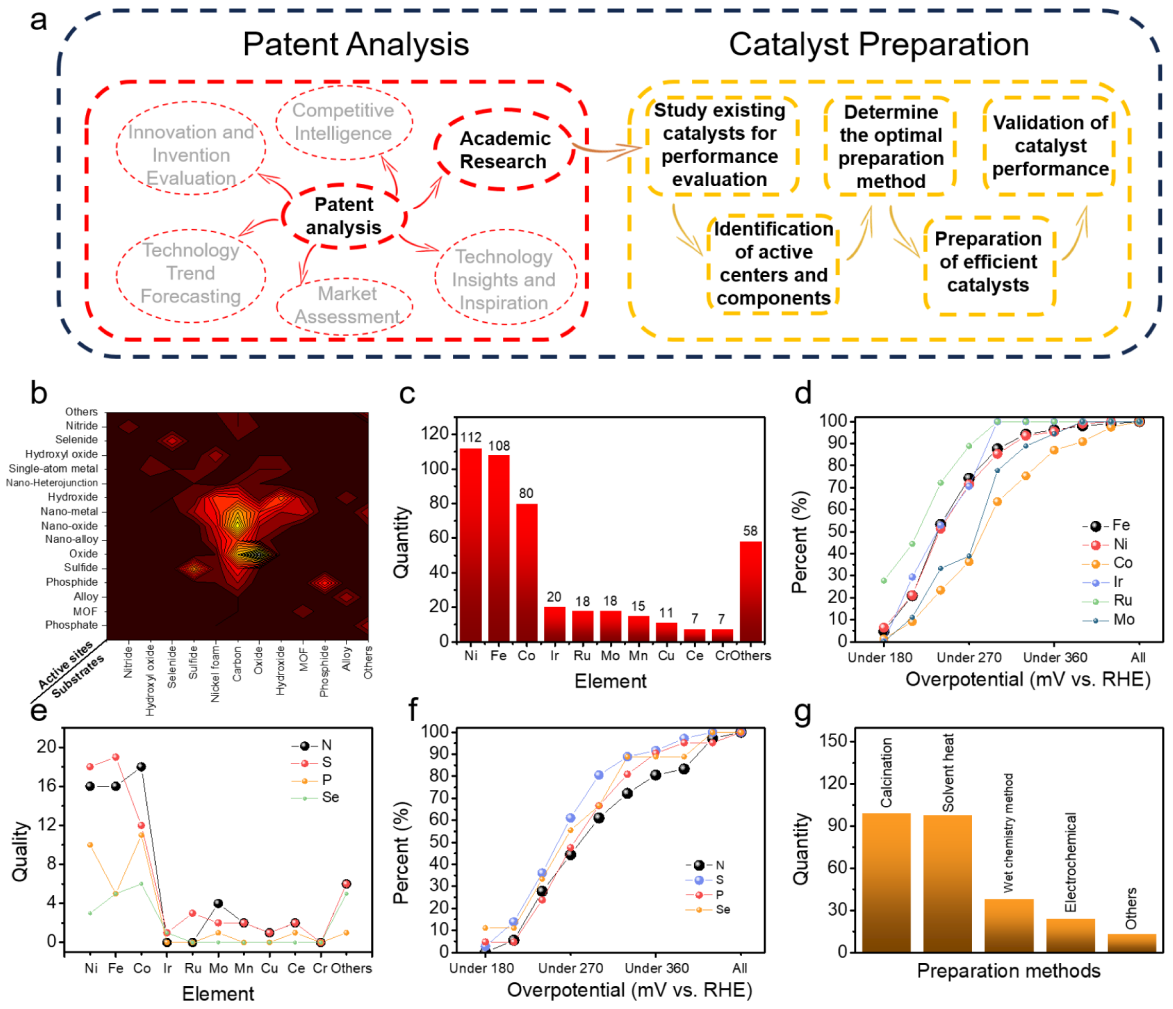

Figure 1. (a) A flowchart of the advantages of PA and the design of catalysts using PA; based on the analysis of published China patents to obtain (b) a volcano plot of substrates and active sites distribution of OER catalysts; (c)a quantity histogram of patents for different metal element doping, (d) percentage distribution of 10 mA cm^{-2} overpotential for doping with different metal elements; (e) the number distribution of patents for different nonmetallic elements doping, (f) a percentage distribution of 10 mA cm^{-2} overpotential for doping with different nonmetallic elements, and (g) quantity histogram of catalysts prepared using different preparation methods.

2. METHOD

2.1. Patent Statistics Process. The searching and categorization of patents are based on the IncoPat platform. In the process of data extraction, for patent samples of different components of catalyst prepared by the same method, we selected samples with better performance and a representative (example) for statistics. For the patents with overpotentials not explicitly given in the original text, we extracted the data directly from the corresponding polarization curve and performed the statistics. For the catalyst preparation time statistics, we do not directly count the key process time given in the patent but also evaluate the period from the beginning to the end of the preparation of the catalyst.

2.2. Synthesis Processes. Nickel(II) nitrate hexahydrate ($Ni(NO_3)_2$ $6H_2O$) (analytical pure); Iron(III) nitrate nonahydrate ($Fe(NO_3)_3$ $9H_2O$) (≥98%); Ruthenium chloride ($RuCl_3$) (Ru content: 45−55%); Ammonium fluoride (NH_3F) (≥98%); Urea (CH_4N_2O) (99.0%−100.5%); Ethylene glycol ($C_2H_6O_2$) (99.8%); Deionized water; Carbon cloth; Potassium hydroxide (KOH); Sulfuric acid (H_2SO_4).

2.2.1. Pretreatment of Carbon Cloth. 160 mL of concentrated H_2SO_4 was uniformly mixed with 40 mL of deionized water to prepare the mixed H_2SO_4 solution. The whole carbon cloth was cut into a number of 2 × 3 cm square small carbon cloth pieces, and they were immersed in the mixed H_2SO_4 solution. After resting for 12 h, the carbon cloth was removed and washed with a lot of deionized water to remove the residual impurities on the surface, dried, and prepared for use.

2.2.2. Preparation of NiFeRu-Carbon. In a typical synthesis, 0.2 g of $Ni(NO_3)_2$ $6H_2O$, 0.1 g of $Fe(NO_3)_3$ $9H_2O$, 0.005 g of $RuCl_3$, 0.2 g of CH_4N_2O and 0.1 g of NH_3F were added to 10 mL of deionized water with ultrasound and mixed in a sonicator for 15 min. The obtained mixed solution was transferred to an autoclave and heated at 130 °C for 12 h. After the reaction was finished, the carbon cloth was removed, rinsed with deionized water, and freeze-dried to obtain NiFeRu-Carbon.

2.2.3. Preparation of NiFe-Carbon. NiFe-Carbon was also synthesized using a recipe similar to that for NiFeRu-Carbon, except that $RuCl_3$ was not added in the preparation of NiFe-Carbon.

2.2.4. Preparation of NiFe/Ru-Carbon. NiFe/Ru-Carbon was synthesized by loading Ru nanoparticles on the NiFe-

https://doi.org/10.1021/acsomega.3c10195
ACS Omega 2024, 9, 18160−18168

Carbon. The detailed method is as follows: the above NiFe-Carbon was prepared in 50 mL of ethylene glycol solution. Then, 1.0 mL Ru^{3+} solution (0.005 mg $RuCl_3$ in 0.1 M HCl solution) was dropped stepwise into the ethylene glycol solution while stirring. The pH of the suspension was adjusted to 11.0 with a 0.1 M NaOH solution, and then the suspension was heated in a microwave oven for 90 s, removed, and cooled to room temperature. Finally, after washing with deionized water and anhydrous ethanol, NiFe/Ru-Carbon was obtained by drying.

2.3. Materials Characterization. Morphological studies were performed by using field emission scanning electron microscopy (SEM) with a Hitachi SU8010 instrument. X-ray diffraction (XRD) analysis was conducted using a Bruker D8 Advance X-ray diffractometer with Cu Kα radiation (λ = 1.5406 Å). X-ray photoelectron spectra (XPS) were obtained using a Thermo Escalab 250XI X-ray photoelectron spectrometer with monochromic Al Ka radiation (hv = 1486.6 eV). Transmission electron microscopy (TEM) images, high-resolution transmission electron microscopy (HRTEM) images, and energy dispersive X-ray spectra (EDS) were acquired using transmission electron microscopy (FEI Tecnai G2 F30) operating at 300 kV. Raman spectra were recorded using a microscopic confocal Raman spectrometer (Renishaw, inVia Reflex) with a wavelength of 514.5 nm. For elemental analysis, inductively coupled plasma mass spectrometry (ICP-MS) was performed on an Agilent cOES730 instrument with argon as the carrier gas.

2.4. Electrochemical Characterization. The electrochemical measurements were conducted by using a VMP3 (BioLogic Inc.) electrochemical workstation. The Nafion D520 solution (5 wt %) utilized in the experiments was procured from DuPont. The Hg/HgO reference electrode and platinum clips were acquired from Tianjin Ida Technology Company. The electrochemical characterization of the OER involved a 1 M KOH solution as the electrolyte within the electrolytic cell. The catalyst carbon cloths employed in the experiments were precisely cut into dimensions of 1 × 1.5 cm and securely affixed using platinum clips, exposing a carbon cloth area of 1 × 1 cm to the electrolyte. LSVs were executed at a scan rate of 10 mV s^{-1} and at room temperature. The OER potential in the *i*R-corrected LSV curves was determined using the equation $E_{\text{Corrected}} = E - iR$, wherein R represents the series resistance obtained from Nyquist plots of electrochemical impedance spectroscopy (EIS).

The TOF was calculated using the following equation:[6]

$$\text{TOF} = \frac{j \times A}{4 \times F \times m}$$

where A is the surface area of the catalytic carbon cloth at the time of the test, j represents the current densities at different overpotentials, m is the number of moles of active sites, and F is the Faraday constant (96485 C mol^{-1}). When calculating the TOF based on the catalyst mass, m is equal to the catalyst mass divided by the relative molecular mass of the catalyst. Here, we calculated TOFs for Ni atoms, Fe atoms, Ru atoms, and all metal atoms as active sites separately.

The volume of the dissolved aqueous O_2 produced was obtained using the drainage method, and the dissolved aqueous OER faradaic efficiency (FE) was calculated for different current densities. The FE was calculated using the following equation:

$$\text{FE}\ (\%) = \frac{n \times F \times V}{Q \times V_m} \times 100\%$$

where n is the number of moles of electrons transferred per 1 mol of O_2 generated, F is the Faraday constant, V is the volume of O_2 generated during water splitting, Q is the electric charge provided by the water splitting process, and V_m is the molar volume of O_2 (22.4 L mol^{-1} at room temperature).

3. RESULT AND DISCUSSION

PA is a method of studying patent documents with the aim of extracting valuable information from patent databases. As shown in Figure 1a, it is widely recognized that the main advantages of PA include: technology trend forecasting,[19] innovation and invention evaluation,[20,21] competitive intelligence,[22] academic research,[23,24] technology transfer,[25] and licensing and market assessment, etc. Of these, we can prepare highly efficient OER catalysts by taking advantage of academic research. Here we collected 205 published patents on the use of OER catalysts in China (Table S1), evaluated the performance and components of these catalysts, and determined the components and preparation methods of novel OER catalysts to prepare highly efficient OER catalysts. Figure 1b is a plot of the volcano profiles of the substrate types and active site types in the patents. It can be seen that carbon is the most used substrate material, with 31.9% of all catalysts using carbon as the substrate material. Although oxides are also commonly used substrate materials, the variety of catalysts that can be designed is limited, and the active sites are often the oxides themselves, such as chalcogenide. The reported metal element doping of the catalysts (Figure 1c) shows that Ni, Fe and Co are the most commonly used metal elements for OER catalysts. While Ir and Ru, although having excellent OER activity by themselves, are much less used than Ni, Fe and Co owing to the scarcity of the precious metals and their high cost. It is worth noting that the nonprecious metal elements, such as Mo and Mn, are also frequently used in the preparation of OER catalysts. The overpotential statistics of the OER catalysts with different metal elements at 10 mA cm^{-2} are shown in Figures 1d and s1. The Ru-containing catalysts exhibited superior overpotentials, with 72% of Ru-containing catalysts exhibiting overpotentials below 240 mV, which is superior to the doping of Fe (53.3%), Ir (52.9%), Ni (51.4%), Mo (33.3%), and Co (23.4%) elements. N, S, P, and Se are nonmetallic elements commonly used in OER catalysts, and Figure 1e shows that these nonmetallic elements are often used to dope nonprecious metal element catalysts to enhance catalytic performance. The nonmetallic elements influence on the activity of the OER catalysts is shown in Figure 1f. The nonmetallic elements have a less significant effect on the overpotential compared to metallic elements. Among the catalysts containing S, 36.1% showed overpotentials below 240 mV, slightly higher than those containing Se (33.3%), N (27.8%), and P (23.8%). In catalyst preparation (Figure 1g), calcination, solvothermal, wet chemistry, and electrochemical methods are the most commonly used approaches for synthesizing the OER catalysts. Among them, calcination and solvothermal methods are widely utilized due to their process stability, but they suffer from the drawback of lengthy preparation cycles, especially when a catalyst is prepared using both solvothermal and calcination techniques, with most processes exceeding 48 h.

https://doi.org/10.1021/acsomega.3c10195
ACS Omega 2024, 9, 18160−18168

Efficient commercial OER catalysts usually need to have the following characteristics: excellent catalytic activity and stability,[26] stable process with a short preparation time, green and nonpolluting,[14] and low cost[26] (Figure 2). Oxides and

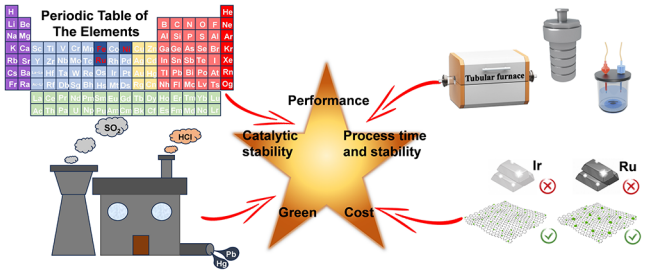

Figure 2. Design concept for highly efficient commercial OER catalysts based on a patent analysis.

hydroxides of NiFe have been extensively studied for their own excellent OER properties and can be used as substrates to provide a stable catalysts. The FeOOH/Ni(OH)$_2$-loaded nickel foam prepared by Bin Wu et al. (CN113026045B) has an overpotential of 280 mV at 500 mA cm^{-2} and remains stable for 250 h. The Ru-based catalysts are highlighted for their activity but are unstable due to the ease of dissolution; for instance, $Y_2Ru_2O_{7-\alpha}$ catalysts prepared by Wang et al. (CN115196696A) are only stable for 10 h. Calcination and solvothermal methods are widely used because of their process stability, but the preparation time is longer, especially when a combination of calcination and solvothermal methods is used. For example, the catalysts invented by Caiqin Li (CN111545207A), Lan Ni (CN111359635A), and Yinling Wang (CN109939685B) have a preparation time of more than 90 h. Electrochemical methods are simple and time-saving, for example, Kong Xiangkai (CN115948762A) can prepare OER catalysts by electrolytic adsorption for 1h. Although the electrochemical method offers a shorter preparation time, it is worth noting that out of the 20 patents filed by various companies, only 2 patents employ the electrochemical approach for participation in the preparation process (electrochemical deposition, CN115369444A; electropolymerization, CN111420692A). This is due to the challenges involved in process control during preparation, making it difficult to achieve large-scale production. The green and sustainable development is the theme of the present era, and the preparation process of efficient OER catalysts should also consider green and pollution-free aspects. Therefore, the design and preparation of catalysts should also take into account avoiding the doping of harmful elements. Although Figure 1f shows that the catalyst doped with the S element has a lower overpotential, the generation of SO_2 or H_2S gas during the preparation process should also be avoided. The premise of large-scale production of OER catalysts is low-cost preparation. Currently, there are two methods for designing low-cost catalysts:[26] (1) replacing noble metal catalysts with non-noble metal catalysts. Qunjie Xu (CN112553643B) successfully synthesized N-doped carbon-coated bimetallic CoMo oxides using Mo as a substitute for noble metals such as Ir and Ru, achieving an overpotential as low as 284 mV at a current density of 10 mA cm^{-2}. (2) Reducing the usage of noble metals through single-atom catalysts or nanoparticle-loaded catalysts. For example, Wang et al. (CN114045524B) designed an Ir single-atom-doped CoOOH catalyst with an overpotential of approximately 270 mV at a current density of 10 mA cm^{-2}. In addition, high-energy-consuming methods, such as calcination or smelting, are not conducive to cost savings. Such as the catalyst invented by Feng Wang (CN115196696A) requires calcination at 1100 °C for 24 h, which consumes an amount of energy.

Based on the PA results provided above, we utilized carbon cloth as the substrate material to ensure excellent electrical conductivity of the catalyst. Subsequently, a one-step hydrothermal method was employed to synthesize NiFeRu-Carbon within a short time frame. The fabrication process of NiFeRu-carbon is shown in Figure 3a. Commercial carbon cloth was

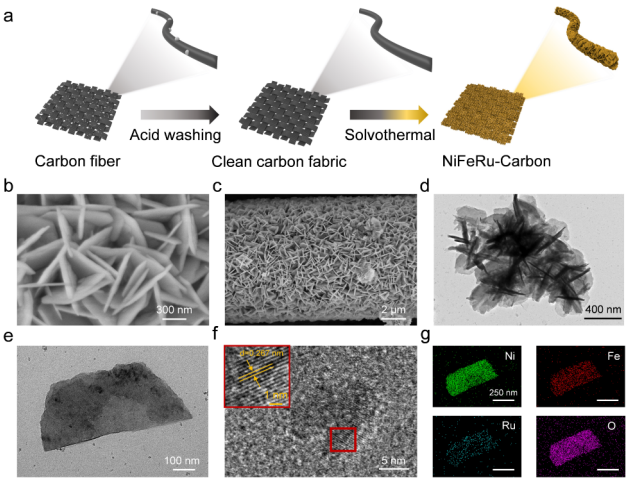

Figure 3. (a) Schematic for the synthesis of NiFeRu-Carbon. (b, c) SEM images and (d, e) TEM images of NiFeRu-Carbon at different magnifications. (f) HRTEM image and (g) EDS mapping spectra of NiFeRu-Carbon.

soaked in concentrated sulfuric acid (H_2SO_4) to remove impurities from the surface of the carbon cloth. The acid-washed, clean carbon cloth was laid flat in an autoclave, and the orange-colored NiFeRu hydroxide was grown on the surface of the carbon fabric by the solvothermal method to obtain NiFeRu-Carbon. To analyze the effect of metal Ru in NiFe substrates on the catalytic properties, we used the same method but with the absence of $RuCl_2$ in the source material to prepare NiFe-loaded carbon cloth (NiFe-Carbon). In addition, Ru was loaded onto NiFe carbon by a microwave reduction method. This resulted in a Ru-doped NiFe carbon cloth (NiFe/Ru-Carbon).

Scanning electron microscopy (SEM) images (Figure 3b,c) of NiFeRu-Carbon show that the NiFeRu hydroxide has a sheet structure and is embedded in the carbon fiber surface without sequence. The thickness was measured to be about 60 nm. Notably, the vertical sheet structure allows full contact with the electrolyte, releasing oxygen to ensure substance exchange. The NiFeRu hydroxide powder (NiFeRu-Powder) was ultrasonically stripped from the NiFeRu-Carbon, and its transmission electron microscopy (TEM) images are shown in Figure 3d,e. The NiFeRu powder is a disordered flowerlike structure, and the length of the sheet was measured to be about 800 nm. High resolution transmission electron microscopy (HRTEM) image (Figure 3f) observes distinct lattice streaks with a lattice spacing of 0.267 nm, corresponding to the (100) crystalline surface of Ni(OH)$_2$.[27] The energy dispersive spectra (EDS) mapping (Figure 3g) reveals that Ni, Fe, Ru, and O are

https://doi.org/10.1021/acsomega.3c10195
ACS Omega 2024, 9, 18160−18168

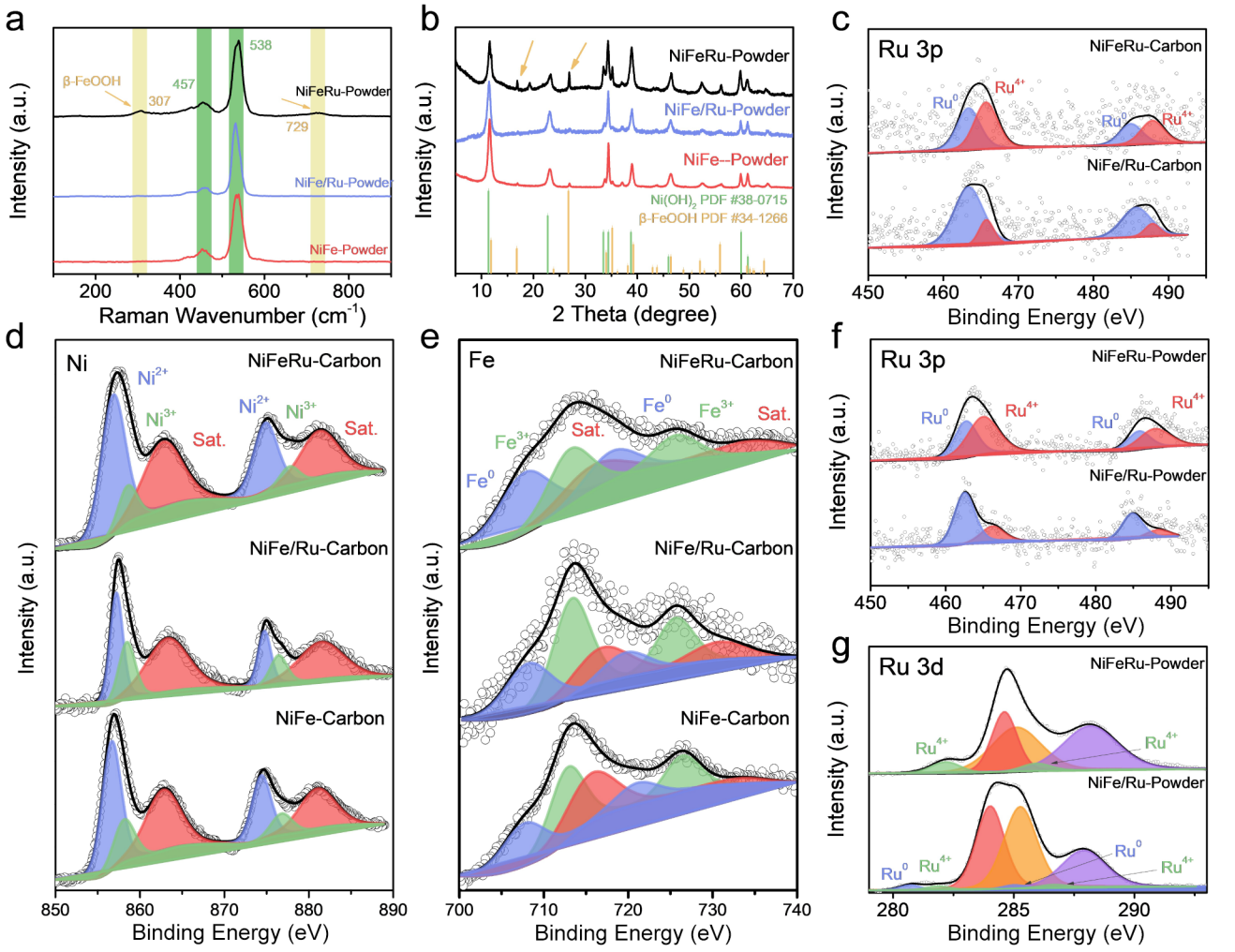

Figure 4. (a) Raman spectra and (b) XRD spectra of NiFeRu-Carbon and comparison samples. (c) XPS Ru 3p, (d) XPS Ni 2p, and (e) XPS Fe 2p spectra of NiFeRu-Carbon and comparison samples. (f) XPS Ru 3p and (g) XPS Ru 3d spectra of NiFeRu-Powder and NiFe/Ru-Powder.

uniformly distributed on the nanosheets. SEM (Figure s2), TEM and EDS mapping (Figure s3) of NiFe/Ru-Carbon and SEM (Figure s4), and TEM and EDS mapping (Figure s5) of NiFe-Carbon show that NiFe/Ru nanosheets and NiFe nanosheets are similar to NiFeRu nanosheets, suggesting that the addition of the metal Ru does not change the morphology of the products. The contents of Ru, Fe, and Ni in the NiFeRu-Powder measured by inductively coupled plasma mass spectrometry (ICP-MS) are 0.3, 15.5, and 39.1 wt %.

NiFeRu-powder, NiFe/Ru-powder, and NiFe-powder were collected for measurement by ultrasound and scraping, which effectively excludes the interference of the carbon substrate in NiFeRu-Carbon, NiFe/Ru-Carbon, and NiFe-Carbon on the analysis of the physical phase. As shown in the Raman spectra of Figure 4a, the spectra of NiFeRe-Powder, NiFe/Re-Powder, and NiFe-Powder all show characteristic peaks of NiFe-layered double hydroxides (NiFe-LDH) at 457 and 538 cm^{-1},[28] indicating that the loadings of the carbon cloth are NiFe-LDH. It is noteworthy that there are two weak peaks at 307 and 729 cm^{-1} in the spectrum of NiFeRu-Powder, which correspond to the characteristic peaks of β-FeOOH.[29,30] In contrast, the characteristic peaks of β-FeOOH were not found in the spectra of the comparison samples, which suggests that the in situ doping of Ru promotes the precipitation of Fe to the surface. The presence of the $Ni(OH)_2$ phase is clearly observed in the X-ray diffraction (XRD) patterns of Figure 4b, and the distinct β-FeOOH phase (PDF #34−1266) is also observed in the pattern of NiFeRu-Powder, which is consistent with the previous results of Raman spectra. X-ray photoelectron spectroscopy (XPS) is used to measure the valence of elements on the surface of a material. The XPS Ru 3p spectra (Figure 4c) of NiFeRu-Carbon and NiFe/Ru-Carbon can be shown as a pair of characteristic Ru^0 peaks at 463.5 and 485.1 eV,[31,32] and a pair of characteristic Ru^{4+} peaks at 465.7 and 487.9 eV.[31,33] The Ru^{4+} peaks of NiFeRu-Carbon are significantly stronger than those of NiFe/Ru-Carbon, which is due to the doping of Ru into the lattice of NiFe-LDH, which provides more electrons for Ni and Fe. And the microwave loading only deposits Ru on the surface of NiFe-LDH, forming more Ru^0 sites. The XPS Ni 2p spectra (Figure 4d) of NiFeRu-Carbon and its comparison samples can be fitted to obtain a pair of strong characteristic peaks of Ni^{2+} at 857.1 and 875.1 eV, and a pair of weak characteristic peaks of Ni^{3+} valence at 858.5 and 877.6 eV.[6,34] The Fe 2p spectra of XPS (Figure 4e) show that the two characteristic Fe^0 peaks are located at 708.3 and 719.1 eV, and the two characteristic Fe^{3+} peaks are located at 713.7 and 716.0 eV.[6,35] The Ni 2p and Fe 2p spectra of NiFeRu-Carbon clearly show that the ratio of low-valent Ni (Ni^{2+}) and low-valent Fe (Fe^0) increases, which may be contributed by the doping of Ru providing electrons to Ni and

https://doi.org/10.1021/acsomega.3c10195
ACS Omega 2024, 9, 18160−18168

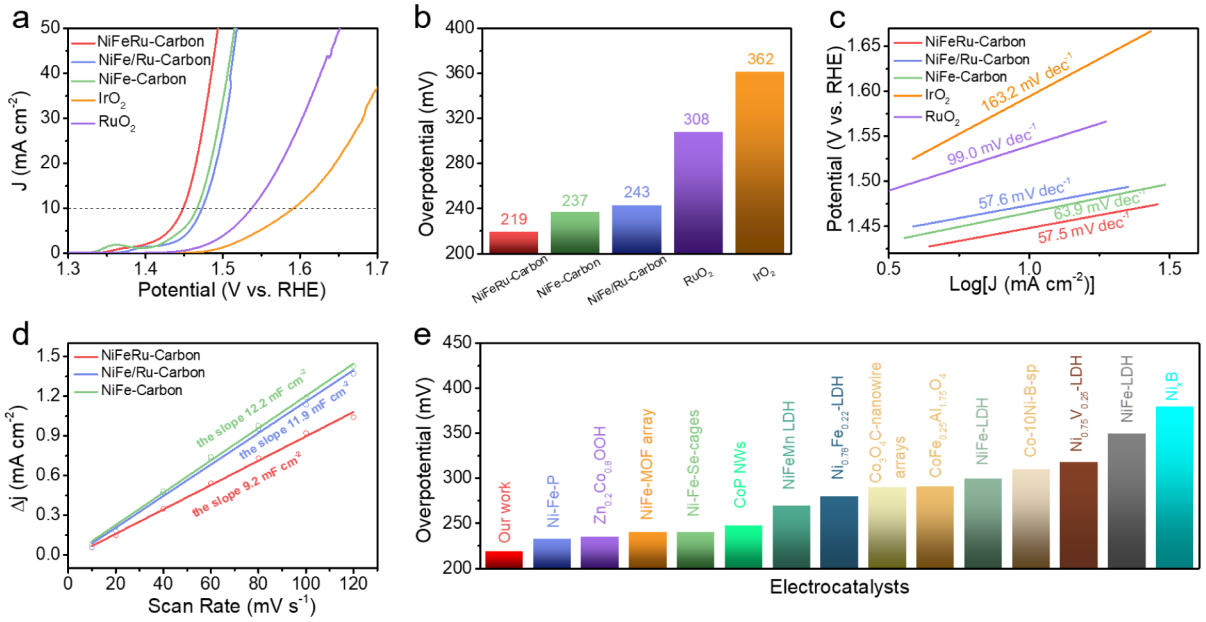

Figure 5. OER catalytic performance was tested using a 1 M KOH electrolyte. (a) Polarization curves, (b) the overpotential for 10 mA cm^{-2}, and (c) the corresponding Tafel plots of NiFeRu-Carbon and comparison samples. (d) Charging current density differences plotted against scan rates. (e) η10 Comparisons of NiFeRu-Carbon and reported excellent OER catalysts.

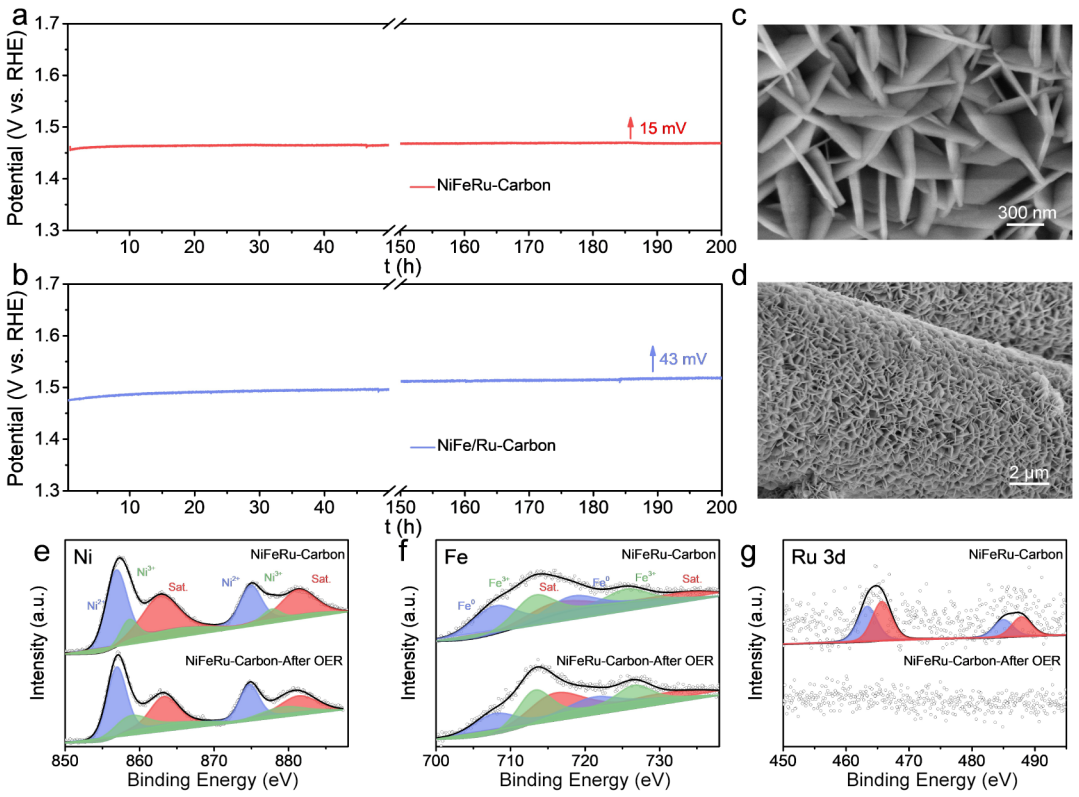

Figure 6. Potentiostatic curve of (a) NiFeRu-Carbon and (b) NiFe/Ru-Carbon at a current density of 10 mA cm^{-2}. (c,d) SEM images of NiFeRu-Carbon after performing the 200 h OER stability test. (e) XPS Ni 2p, (f) XPS Fe 2p, and (g) XPS Ru 3d comparison spectra of NiFeRu-Carbon before and after performing the 200 h OER stability test.

Fe and occupying the lattice of NiFe-LDH, resulting in the precipitation of part of the Fe elements onto the double hydroxides surface. This result is also consistent with the Raman spectra and XRD. The XPS Ru 3d spectrum is overlapped with the C 1s spectrum, and in order to exclude the interference of the carbon substrate, NiFeRu-Powder and NiFe/Ru-Powder were reexamined for the XPS spectra of Ru. XPS Ru 3p spectra of NiFeRu-Powder still reveal a high Ru^{4+} occupancy, while NiFe/Ru-Powder has a higher Ru^{0} ratio, which is consistent with the results of Figure 4f. XPS Ru 3d spectra (Figure 4g) of NiFeRu-Powder reveal weak two peaks at 282.2 and 286.0 eV, which correspond to Ru^{4+}.[31,36] Whereas

https://doi.org/10.1021/acsomega.3c10195
ACS Omega 2024, 9, 18160−18168

the Ru 3d spectra of NiFe/Ru-Powder show the presence of two peaks at much lower energy (280.7 and 285.0 eV), which correspond to the Ru^0.[31,36] The more high-valent Ru in the NiFeRu-Carbon is again confirmed.

The electrocatalytic activity of NiFeRu-Carbon toward the OER was evaluated in a 1 M KOH solution in a standard three-electrode electrochemical cell. The Hg/HgO electrode was the reference electrode, and Pt foil was the counter electrode. Also, NiFe/Ru-Carbon, NiFe-Carbon, commercial RuO_2, and commercial IrO_2 were measured as OER reaction catalysts for comparison with NiFeRu-Carbon. The polarization curves of NiFeRu-Carbon and comparison catalysts are shown in Figure 5a. Among the five catalysts, the OER onset potential of NiFeRu-Carbon is the lowest, indicating the highest catalytic activity. Furthermore, the comparison of the overpotentials at 10 mA cm^{-2} (η10) (Figure 5b) shows that NiFeRu-Carbon had the lowest η10 (219 mV), which was superior to those of NiFeRu-Carbon (243 mV), NiFe-Carbon (237 mV), commercial RuO_2 (308 mV), and commercial IrO_2 (362 mV). Tafel plots resulting from the polarization curves for the different catalysts are given in Figure 5c. The lowest Tafel slope (57.5 mV dec^{-1}) was observed for NiFeRu-Carbon, indicating superior OER kinetics.[37] At a slower scan rate (2 mV s^{-1}), NiFeRu-Carbon also exhibits excellent catalytic activity (Figure s6), with a η10 of 215 mV, which is superior to that of the other comparison samples. NiFeRu-Carbon and comparison catalysts were performed by cyclic voltammetry (CV) at different scan rates (10, 20, 40, 60, 80, 100, and 120 mV s^{-1}), and the results are shown in Figures 5d and s7. The linear slope is equivalent to twice the C_{dl}, and also indicates the minimum electrochemical active surface area (ECSA) for NiFeRu-Carbon.[6] We calculated the TOFs of NiFeRu-Carbon and NiFe-Carbon, assuming that all the metal sites were involved in the OER. The results (Figure s8) show that the TOFs of Ni and Fe in NiFeRu-LDH are higher than those of NiFe-LDH at overpotentials of 200 mV, 240 mV, and 280 mV, which suggests that the atomic utilization efficiency of Ni and Fe in NiFeRu-LDH is more efficient and the unit activity is higher after doping with a small amount of Ru. The results for the OER faradaic efficiency (FE) are shown in Figure s9. The volume of O_2 produced was measured to be 2.5 mL, 3.4 mL, and 4.4 mL, respectively, after 300 s of reaction at current densities of 150 mA cm^{-2}, 200 mA cm^{-2}, and 250 mA cm^{-2}. Therefore, the FEs of the O_2 production from NiFeRu-Carbon were calculated to be 95.7%−101.1% (Figure s9b), and the results indicate that NiFeRu-Carbon has high OER efficiency in alkaline electrolyte. It is noteworthy that NiFeRu-Carbon exhibits the lowest η10 and the smallest ECSA among the studied materials, indicating the highest intrinsic activity of individual catalytic sites within NiFeRu-Carbon. The OER activities of NiFeRu-Carbon were also compared with those of the reported excellent OER catalysts, and it was found that our catalyst has the highest efficiency with a low η10 of 219 mV (Figure 5e and Table s2).

In order to investigate the stability of the OER process for NiFeRu-Carbon, we performed potentiostatic curve tests at a 10 mA cm^{-2} overpotential, and NiFe/Ru-Carbon was also tested as the reference sample. Figure 6a,b show that after 200 h of operation, the overpotential of NiFeRu-Carbon at 10 mA cm^{-2} increases by only 15 mV, whereas the overpotential of NiFe/Ru-Carbon increases by 43 mV, and NiFeRu-Carbon shows more superior OER stability. Moreover, SEM images (Figure 6c,d) showed that loadings of NiFeRu-Carbon remained sheet structure and stably embedded on carbon fibers after a 200 h OER stability test, and there was no change in the morphology of NiFeRu-Carbon before and after the OER. Compare the XPS of NiFeRu-Carbon before and after the OER to analyze the change in elemental valence. The Ni 2p spectra (Figure 6e) showed that the valence state of Ni did not change significantly after OER stability testing. The Fe 2p spectra (Figure 6f) showed that the proportion of Fe^{3+} became obviously higher after the OER reaction, which may be owing to Fe acted as the active site during the OER process and Fe^0 was oxidized to Fe^{3+}.[3,38] The Ru 3d spectra (Figure 6g) show that Ru in NiFeRu-Carbon is not detected after a long OER test, which may be due to the dissolution of Ru elements in NiFeRu-LDH, which generates a large number of oxygen vacancies in NiFeRu-LDH,[39,40] allowing NiFeRu-Carbon to maintain excellent OER performance. The EPR test is used to verify the formation of oxygen vacancies (Figure s10). The results show that NiFeRu-Carbon has a strong O_V feature signal around g = 2.003, especially the O_V feature signal intensity is higher after a long time $V-t$ test, which suggests that the content of oxygen vacancies in NiFeRu-Carbon is enhanced. This result is consistent with the XPS results and confirms our conclusion.

4. CONCLUSION

In summary, employing a patent analysis approach, we inferred the type and composition of efficient oxygen evolution reaction (OER) catalysts and expediently synthesized a high-performance NiFeRu-Carbon catalyst through a facile one-step hydrothermal method. This catalyst exhibits a relatively low Ru loading (0.3 wt %), yet achieves an overpotential of 219 mV at 10 mA cm^{-2} current density in alkaline electrolyte, and following a stability test of 200 h, the overpotential experiences a mere attenuation of 15 mV. Importantly, upon characterization of samples before and after stability testing, the dissolution of Ru was observed, introducing a significant number of oxygen vacancies that enhance the stability of NiFe-LDH.

■ ASSOCIATED CONTENT

Supporting Information

The Supporting Information is available free of charge at https://pubs.acs.org/doi/10.1021/acsomega.3c10195.

Patent number distribution of different metal catalysts at 10 mA cm^{-2} overpotential; SEM, TEM, and EDS pictures of NiFe/Ru-Carbon and NiFe-Carbon catalysts; polarization curves and the overpotential of NiFeRu-Carbon and comparison samples at the scan rate of 2 mV s^{-1}; CV curves for different catalysts at different scan rates; comparison of TOFs of NiFeRu-Carbon and NiFe-Carbon; Faradaic efficiency and EPR spectra of NiFeRu-Carbon; list of collected OER patents; comparison of OER activity with reported catalysts (PDF)

■ AUTHOR INFORMATION

Corresponding Authors

Baorui Jia − *Institute for Advanced Materials and Technology, University of Science and Technology Beijing, Beijing 100083, China;* orcid.org/0000-0002-1846-6971; Email: jiabaorui@ustb.edu.cn

Wujun Zhang − *School of Economics and Management, University of Science and Technology Beijing, Beijing 100083,*

https://doi.org/10.1021/acsomega.3c10195
ACS Omega 2024, 9, 18160−18168

China; Intellectual Property Research Center, University of Science and Technology Beijing, Beijing 100083, China; Email: zhangwujun@ustb.edu.cn

Mingli Qin − *Institute for Advanced Materials and Technology, University of Science and Technology Beijing, Beijing 100083, China; Beijing Advanced Innovation Center for Materials Genome Engineering, University of Science and Technology Beijing, Beijing 100083, China; Institute of Materials Intelligent Technology, Liaoning Academy of Materials, Shenyang 110004, China;* orcid.org/0000-0002-4001-6539; Email: qinml@mater.ustb.edu.cn

Authors

Weiwei Zhang − *School of Economics and Management, University of Science and Technology Beijing, Beijing 100083, China*

Yongzhi Zhao − *Institute for Advanced Materials and Technology, University of Science and Technology Beijing, Beijing 100083, China*

Jiali Xu − *School of Economics and Management, University of Science and Technology Beijing, Beijing 100083, China; Intellectual Property Research Center, University of Science and Technology Beijing, Beijing 100083, China*

Complete contact information is available at: https://pubs.acs.org/10.1021/acsomega.3c10195

Author Contributions

#W.Z. and Y.Z. contributed equally to this manuscript.

Notes

The authors declare no competing financial interest.

■ ACKNOWLEDGMENTS

The authors gratefully acknowledge financial support from the National Key Research and Development Program of China (2022YFB3708800, 2021YFB3701900), National Natural Science Foundation Program of China (52131307, 52071013, and 52174344), Beijing Municipal Science & Technology Commission, Administrative Commission of Zhongguancun Science Park (Z221100005822001), the Natural Science Foundation Program of Beijing (2224104 and 2162027), Guangdong Basic and Applied Basic Research Foundation (2023A1515140193), the Fundamental Research Funds for the Central Universities (FRF-IDRY-GD21-002, FRF-TP-19-003C2, and FRF-IPPE-2207), and China Scholarship Council Foundation Program (202206460033).

■ REFERENCES

(1) Jothi, V. R.; Bose, R.; Rajan, H.; Jung, C.; Yi, S. C. Harvesting electronic waste for the development of highly efficient eco-design electrodes for electrocatalytic water splitting. *Adv. Energy Mater.* **2018**, *8* (34), 1802615.

(2) Yu, M.; Budiyanto, E.; Tüysüz, P. D. H. Principles of water electrolysis and recent progress in cobalt-, nickel-, and iron-based oxides for the oxygen evolution reaction. *Angew. Chem., Int. Ed.* **2022**, *61* (1), No. e202103824.

(3) Wang, Y.; Zhao, Y.; Liu, L.; Qin, W.; Liu, S.; Tu, J.; Liu, Y.; Qin, Y.; Liu, J.; Wu, H.; Zhang, D.; Chu, A.; Jia, B.; Qu, X.; Qin, M.; Xue, J. Facet Engineering and Pore Design Boost Dynamic Fe Exchange in Oxygen Evolution Catalysis to Break the Activity−Stability Trade-Off. *J. Am. Chem. Soc.* **2023**, *145*, 20261−20272.

(4) Wang, J.; Zhou, X.; Li, B.; Yang, D.; Lv, H.; Xiao, Q.; Ming, P.; Wei, X.; Zhang, C. Highly efficient, cell reversal resistant PEMFC based on PtNi/C octahedral and OER composite catalyst. *Int. J. Hydrogen Energy* **2020**, *45*, 8930−8940.

(5) Mladenović, D.; Mladenović, A.; Santos, D. M. F.; Yurtcan, A. B.; Miljanić, ˇ.; Mentus, S.; šljukić, B. Transition metal oxides for bifunctional ORR/OER electrocatalysis in unitized regenerative fuel cells. *Electroanal. Chem.* **2023**, *946*, 117709.

(6) Wang, Y.; Zhao, Y.; Liu, L.; Qin, W.; Liu, S.; Tu, J.; Qin, Y.; Liu, J.; Wu, H.; Zhang, D.; Chu, A.; Jia, B.; Qu, X.; Qin, M. Mesoporous single crystals with Fe-rich skin for ultralow overpotential in oxygen evolution catalysis. *Adv. Mater.* **2022**, *34* (20), 2200088.

(7) Zhao, Y.; Zhang, Z.; Liu, L.; Wang, Y.; Wu, T.; Qin, W.; Liu, S.; Jia, B.; Wu, H.; Zhang, D.; Qu, X.; Qi, G.; Giannelis, E. P.; Qin, M.; Guo, S. S and O Co-Coordinated Mo Single Sites in Hierarchically Porous Tubes from Sulfur−Enamine Copolymerization for Oxygen Reduction and Evolution. *J. Am. Chem. Soc.* **2022**, *144*, 20571−20581.

(8) Yin, J.; Jin, J.; Liu, H.; Huang, B.; Lu, M.; Li, J.; Liu, H.; Zhang, H.; Peng, Y.; Xi, P.; Yan, C. NiCo 2 O 4 -Based Nanosheets with Uniform 4 nm Mesopores for Excellent Zn−Air Battery Performance. *Adv. Mater.* **2020**, *32* (39), 2001651.

(9) Fu, J.; Cano, Z. P.; Park, M. G.; Yu, A.; Fowler, M.; Chen, Z. Electrically Rechargeable Zinc−Air Batteries: Progress, Challenges, and Perspectives. *Adv. Mater.* **2017**, *29* (7), 1604685.

(10) Amiinu, I.; Pu, Z.; Liu, X.; Owusu, K. A.; Monestel, H. G. R.; Boakye, F. O.; Zhang, H.; Mu, S. Multifunctional Mo−N/C@MoS $_2$ Electrocatalysts for HER, OER, ORR, and Zn−Air Batteries. *Adv. Funct. Mater.* **2017**, *27* (44), 1702300.

(11) Roy, A.; Jadhav, H. S.; Cho, M.; Seo, J. G. Electrochemical deposition of self-supported bifunctional copper oxide electrocatalyst for methanol oxidation and oxygen evolution reaction. *J. Ind. Eng. Chem.* **2019**, *76*, 515−523.

(12) Beni, G.; Schiavone, L. M.; Shay, J. L.; Dautremont-Smith, W. C.; Schneider, B. S. Electrocatalytic oxygen evolution on reactively sputtered electrochromic iridium oxide films. *Nature* **1979**, *282*, 281−283.

(13) Trotochaud, L.; Mills, T. J.; Boettcher, S. W. An optocatalytic model for semiconductor−catalyst water-splitting photoelectrodes based on in situ optical measurements on operational catalysts. *J. Phys. Chem. Lett.* **2013**, *4*, 931−935.

(14) Zeng, K.; Zheng, X.; Li, C.; Yan, J.; Tian, J.; Jin, C.; Strasser, P.; Yang, R. Recent advances in non-noble bifunctional oxygen electrocatalysts toward large-scale production. *Adv. Funct. Mater.* **2020**, *30* (27), 2000503.

(15) Chen, F.; Wu, Z.; Adler, Z.; Wang, H. Stability challenges of electrocatalytic oxygen evolution reaction: From mechanistic understanding to reactor design. *Joule* **2021**, *5*, 1704−1731.

(16) Devarajan, B.; Saravanakumar, R.; Sivalingam, S.; Bhuvaneswari, V.; Karimi, F.; Rajeshkumar, L. Catalyst derived from wastes for biofuel production: A critical review and patent landscape analysis. *Appli. Nanosci.* **2022**, *12*, 3677−3701.

(17) Stoffels, M. A.; Klauck, F. J. R.; Hamadi, T.; Glorius, F.; Leker, J. Technology trends of catalysts in hydrogenation reactions: A patent landscape analysis. *Adv. Synth. Catal.* **2020**, *362*, 1258−1274.

(18) Jun, S.; Park, S. S. Examining technological innovation of Apple using patent analysis. *Ind. Manage. Data Syst.* **2013**, *113* (6), 890−907.

(19) Albino, V.; Ardito, L.; Dangelico, R. M.; Petruzzelli, A. M. Understanding the development trends of low-carbon energy technologies: A patent analysis. *Appl. Energy* **2014**, *135*, 836−854.

(20) Barcelon, Y. C. Role of patent analysis in corporate R&D. *Pharm. Pat. Anal.* **2012**, *1*, 5−7.

(21) Abraham, B. P.; Moitra, S. D. Innovation assessment through patent analysis. *Technovation* **2001**, *21*, 245−252.

(22) Yang, X.; Yu, X.; Liu, X. Obtaining a sustainable competitive advantage from patent information: A patent analysis of the graphene industry. *Sustainability* **2018**, *10*, 4800.

(23) Van Zeebroeck, N.; Van Pottelsberghe de la Potterie, B.; Guellec, D. Patents and academic research: A state of the art. *J. Intellect. Cap.* **2008**, *9* (2), 246−263.

(24) Aithal, P. S.; Aithal, S. Patent analysis as a new scholarly research method. *Int. J. Case Stud. Bus. IT Educ.* **2018**, *2*, 33−47.

(25) Park, H.; Yoon, J.; Kim, K. Using function-based patent analysis to identify potential application areas of technology for technology transfer. *Expert Syst. Appl.* **2013**, *40*, 5260−5265.
(26) Yoon, H.; Ju, B.; Kim, D. W. Perspectives on the development of highly active, stable, and cost-effective OER electrocatalysts in acid. *Battery Energy* **2023**, *2* (5), 20230017.
(27) Dong, Z.; Lin, F.; Yao, Y.; Jiao, L. Crystalline Ni $(OH)_2$/amorphous $NiMoO_x$ mixed-catalyst with Pt-like performance for hydrogen production. *Adv. Energy Mater.* **2019**, *9* (46), 1902703.
(28) Wu, Z.; Zou, Z.; Huang, J.; Gao, F. $NiFe_2O_4$ nanoparticles/NiFe layered double-hydroxide nanosheet heterostructure array for efficient overall water splitting at large current densities. *ACS Appl. Mater. Interfaces* **2018**, *10*, 26283−26292.
(29) Li, Y.; Wu, Y.; Yuan, M.; Hao, H.; Lv, Z.; Xu, L.; Wei, B. Operando spectroscopies unveil interfacial FeOOH induced highly reactive β-Ni(Fe)OOH for efficient oxygen evolution. *Appl. Catal., B* **2022**, *318*, 121825.
(30) Hu, L.; Li, S.; Chu, J.; Niu, S.; Wang, J.; Du, Y.; Li, Z.; Han, X.; Xu, P. Understanding the phase-induced electrocatalytic oxygen evolution reaction activity on FeOOH nanostructures. *ACS Catal.* **2019**, *9*, 10705−10711.
(31) Wang, H.; Li, X.; Ruan, Q.; Tang, J. Ru and RuO_x decorated carbon nitride for efficient ammonia photosynthesis. *Nanoscale* **2020**, *12*, 12329−12335.
(32) Qin, X.; Zhang, L.; Xu, G.; Zhu, S.; Wang, Q.; Gu, M.; Zhang, X.; Sun, C.; Balbuena, P. B.; Amine, K.; Shao, M. The role of Ru in improving the activity of Pd toward hydrogen evolution and oxidation reactions in alkaline solutions. *ACS Catal.* **2019**, *9*, 9614−9621.
(33) Liu, S.; Yu, B.; Wang, Z.; Hu, J.; Fu, M.; Wang, Y.; Liu, J.; Guo, Z.; Xu, X.; Ding, Y. Highly selective isomerization of cottonseed oil into conjugated linoleic acid catalyzed by multiwalled carbon nanotube supported ruthenium. *RSC Adv.* **2019**, *9*, 20698−20705.
(34) Cheng, M.; Fan, H.; Song, Y.; Cui, Y.; Wang, R. Interconnected hierarchical $NiCo_2O_4$ microspheres as high-performance electrode materials for supercapacitors. *Dalton Trans.* **2017**, *46*, 9201−9209.
(35) Hou, Z.; Yan, P.; Sun, B.; Elshekh, H.; Yan, B. An excellent soft magnetic Fe/Fe_3O_4-FeSiAl composite with high permeability and low core loss. *Results Phys.* **2019**, *14*, 102498.
(36) Lao, M.; Zhao, G.; Li, P.; Ma, T.; Jiang, Y.; Pan, H.; Dou, S.; Sun, W. Manipulating the Coordination Chemistry of Ru-N(O)-C Moieties for Fast Alkaline Hydrogen Evolution Kinetics. *Adv. Funct. Mater.* **2021**, *31* (33), 2100698.
(37) Zhao, Y.; Wu, H.; Wang, Y.; Liu, L.; Qin, W.; Liu, S.; Liu, J.; Qin, Y.; Zhang, D.; Chu, A.; Jia, B.; Qu, X.; Qin, M. Sulfur coordination engineering of molybdenum single-atom for dual-functional oxygen reduction/evolution catalysis. *Energy Storage Mater.* **2022**, *50*, 186−195.
(38) Wang, Y.; Zhang, X.; Huang, L.; Guo, Y.; Yuan, X.; Hou, H.; Wu, J.; Lu, C.; Zhang, Y. Electrooxidation-enabled electroactive high-valence ferritic species in NiFe layered double hydroxide arrays as efficient oxygen evolution catalysts. *J. Colloid Interface Sci.* **2021**, *599*, 168−177.
(39) Zhang, L.; Jang, H.; Liu, H.; Kim, M. G.; Yang, D.; Liu, S.; Liu, X.; Cho, J. Sodium-decorated amorphous/crystalline RuO_2 with rich oxygen vacancies: a robust pH-universal oxygen evolution electrocatalyst. *Angew. Chem., Int. Ed.* **2021**, *133*, 18969−18977.
(40) Li, Q.; Huang, F.; Li, S.; Zhang, H.; Yu, X. Oxygen Vacancy Engineering Synergistic with Surface Hydrophilicity Modification of Hollow Ru Doped CoNi-LDH Nanotube Arrays for Boosting Hydrogen Evolution. *Small* **2022**, *18* (2), 2104323.

https://doi.org/10.1021/acsomega.3c10195
ACS Omega 2024, 9, 18160−18168